Comparative numerical integration of simple atmospheric models on a spherical grid[1]

By W. LAWRENCE GATES[2] and CHRISTOPHER A. RIEGEL, *University of California, Los Angeles*

(Manuscript received June 13, 1963)

ABSTRACT

The non-divergent barotropic model, the two-layer quasi-geostrophic baroclinic model, and the two-layer balanced baroclinic model of variable static stability are integrated in parallel on a spherical grid with comparable boundary and initial conditions for the case of 00 GCT,[3] 7 December 1957. The integrations of the barotropic and quasi-geostrophic models show the expected accuracy decay to 72 hr, characterized by excessive momentum transport into the jet and an overall failure to predict significant baroclinic development. The balanced model displays an initially similar behavior, although the vertical motions are about twice those of the quasi-geostrophic case. Beyond 12 hr the balanced model's vertical motions become excessively cellular and of increased magnitude, and a progressively serious distortion of the solutions takes place by 24 hr. The energy transformations of the variable-stability model indicate a disturbance evolution significantly different from that of the quasi-geostrophic model, although beyond 12 hr these transformations are themselves seriously influenced by the computed vertical motions. A number of recommendations for further tests are made, of which the improvement of the finite-difference schemes is probably the most important.

1. Introduction

In the effort to obtain effective dynamic models for the short-range numerical prediction of large-scale atmospheric flow, the number of models proposed has always been larger than the number of models subjected to systematic test. The adequate testing of a prediction model is demanding and time-consuming work, and cannot be successfully undertaken without access to appropriate computing facilities. Moreover, each of the prediction models proposed need not be exhaustively tested, but only those seemingly representing significantly different characteristics. Taking a broad view of the dynamic modeling problem, we may note three major classes: (i) quasi-geostrophic models (ii) balanced or filtered models and (iii) primitive models. In each of these divisions, we may envisage a barotropic model and a series of baroclinic models of increasing vertical resolution, and a comprehensive testing program should include representatives from each class.

The relatively limited testing programs undertaken heretofore have usually concentrated on the performance of a single model in comparison with synoptic or conventional prediction techniques. Among the more prominent of such tests are those of the barotropic model made at the International Meteorological Institute in Stockholm (Bolin, 1955; Döös, 1962), those by the Joint Numerical Weather Prediction Unit in Washington (Bolin *et al.* 1962), and those made by the German Weather Service in Frankfurt (Bolin *et al.*, 1962). Simple baroclinic models have also been tested against conventional synoptic forecasts by the British Meteorological Office (Bushby & Hinds, 1955; Knighting & Hinds, 1960; Knighting, Corby, Bushby & Wallington, 1961).

Quite aside from the obvious practical importance of such tests, it is the *comparative* performance of two or more dynamic models under the same conditions which reveals their relative abilities (or lack of them), and upon which con-

---

[1] Presented at the WMHO/IUGG Symposium on Numerical Weather Forecasting, Oslo 1963.

[2] Now at The Travelers Research Center, Inc., Hartford, Conn.

[3] GCT = Greenwich Civil Time = GMT.

clusions of model superiority must be based. There appear to have been relatively few tests of this kind; the most comprehensive are the tests of the barotropic model and of a baroclinic primitive equation model made by the German Weather Service (Staff Members, Deutscher Wetterdienst, 1960; EDELMANN & REISER, 1962). Earlier and somewhat more limited tests of various versions of the barotropic model have been reported by BOLIN (1956) and CRESSMAN (1958, 1960), while comparison of a barotropic and a 2-level baroclinic model has been made at the Air Force Cambridge Research Center (GATES *et al.*, 1955; THOMPSON & GATES, 1956). More recently, comparative tests of two- and three-parameter models have been made at the British Meteorological Office (BUSHBY & WHITELAM, 1961; KNIGHTING, 1962).

In the present paper we shall consider the results of some new comparative numerical integrations for a barotropic model, a two-level quasi-geostrophic model, and a two-level balanced model. These tests were made over the hemisphere by as nearly comparable numerical procedures as possible, in an effort to permit a meaningful inter-model comparison in the test case selected. No attempt has been made in this series to test a representative of the primitive models, nor have baroclinic models with more than two levels been examined.

2. The barotropic model

The barotropic model examined in the present tests is that for horizontal and non-divergent flow. In terms of a streamfunction ψ, this model is represented by the vorticity equation

$$\nabla^2\left(\frac{\partial\psi}{\partial t}\right) + J(\psi, \nabla^2\psi + f) = 0, \tag{1}$$

where ∇^2 is the horizontal (isobaric) Laplace operator, J the Jacobian operator, and f the Coriolis parameter. Here the streamfunction ψ would normally be found from the balance equation

$$f\nabla^2\psi + \beta\frac{\partial\psi}{\partial y} - 2J\left(\frac{\partial\psi}{\partial x}, \frac{\partial\psi}{\partial y}\right) = \nabla^2\phi, \tag{2}$$

where $\beta = \partial f/\partial y$ and ϕ is the geopotential. In the present case, however, (2) is approximated by

$$\nabla\cdot(f\nabla\psi) = \nabla^2\phi, \tag{3}$$

where ∇ is the horizontal gradient operator. This represents the neglect of the non-linear Jacobian term in (2), and (3) may therefore be termed the linear balance equation. While the use of (3) rather than (2) obviously simplifies the computation of ψ from known ϕ, it has deliberately been used here in order to make the barotropic ψ comparable with the streamfunction of the two-level balanced model for which a relation of the form (3) is to be specified.

3. The two-level quasi-geostophic model

This model is the simplest and most familiar of the baroclinic models employing the quasi-geostrophic approximation. Here the vorticity equation is used in the form

$$\nabla^2\left(\frac{\partial\phi}{\partial t}\right) + J(\phi, \zeta + f) - f_0^2\frac{\partial\omega}{\partial p} = 0, \tag{4}$$

where $\omega = dp/dt$, and f_0 is an average (constant) value of the Coriolis parameter consistent with the quasi-geostrophic approximations

$$\mathbf{v}_H = f_0^{-1}\mathbf{k}\times\nabla\phi, \quad \zeta = f_0^{-1}\nabla^2\phi. \tag{5}$$

Accompanying (4) are the adiabatic, continuity, and hydrostatic equations in the usual forms,

$$\frac{\partial\theta}{\partial t} + \mathbf{v}_H\cdot\nabla\theta + \omega\frac{\partial\theta}{\partial p} = 0, \tag{6}$$

$$\frac{\partial\omega}{\partial p} + \nabla^2\chi = 0, \tag{7}$$

$$\frac{\partial\phi}{\partial p} + \frac{RT}{p} = 0, \tag{8}$$

where θ is the potential temperature, T the absolute temperature, and χ is the velocity potential (for the divergent wind component). According to the quasi-geostrophic approximation, $\mathbf{v}_H$ in (6) is to be found from (5), and $\partial\theta/\partial p$ assigned a constant value in x and y.

Dividing the atmosphere into four equal layers or pressure increments of $p_0/4$, using centered finite differences to evaluate the (first) pressure derivatives with the boundary conditions $\omega = 0$ at $p = 0$, p_0 (1000 mb), we find the system

$$\nabla^2\left(\frac{\partial\psi}{\partial t}\right) + J(\psi, \nabla^2\psi + f) + J(\tau, \nabla^2\tau) = 0, \quad (9)$$

$$\nabla^2\left(\frac{\partial\tau}{\partial t}\right) + J(\tau, \nabla^2\psi + f) + J(\psi, \nabla^2\tau) - \frac{2f_0}{p_0}\omega = 0, \quad (10)$$

$$\sigma_0\nabla^2\omega - 2^\varkappa f_0^2 R^{-1}\omega = \frac{p_0}{4}\nabla^2 J(\psi, \theta) - \frac{2^{\varkappa-1} f_0 p_0}{R}[J(\tau, \nabla^2\psi + f) + J(\psi, \nabla^2\tau)], \quad (11)$$

$$\theta = 2^{\varkappa+1} f_0 R^{-1}\tau. \quad (12)$$

Here the new dependent variables are defined as

$$\psi = (\phi_1 + \phi_3)(2f_0)^{-1}, \quad (13)$$

$$\tau = (\phi_1 - \phi_3)(2f_0)^{-1}, \quad (14)$$

$$\theta = \theta_2, \quad (15)$$

$$\omega = \omega_2. \quad (16)$$

where the subscripts 1, 2, 3 denote evaluation at the levels $p_0/4$, $p_0/2$, $3p_0/4$ respectively, and $\sigma_0 = (\partial\theta/\partial p)_2$ is the constant static stability. Equations (9) and (10) are forms of the so-called mean and thermal vorticity equations, respectively, (11) is the 2-level ω-equation, and (12) is a form of the thermal wind relation.

4. The two-layer balanced model of variable static stability

This model represents a generalization of the two-level model just considered (§ 3) in the following respects: (i) the static stability is allowed to freely vary in x, y and t, (ii) the advection of temperature by the divergent wind is included, and (iii) the Coriolis parameter is allowed full variability. Such a model has been derived by Lorenz (1960), and represents an energetically more consistent formulation than does the quasi-geostrophic case. Writing the horizontal wind as

$$\mathbf{v}_H = \mathbf{k} \times \nabla\psi + \nabla\chi, \quad (17)$$

where ψ is a streamfunction for the non-divergent part of $\mathbf{v}_H$ and χ is the potential function for the irrotational part, the vorticity $\zeta = \nabla^2\psi$ and the (horizontal) divergence $\delta = \nabla^2\chi$. In these notations the quasi-geostrophic vorticity equation (4) is replaced by the balance vorticity equation

$$\nabla^2\left(\frac{\partial\psi}{\partial t}\right) + J(\psi, \nabla^2\psi + f) + \nabla\cdot(f\nabla\chi) = 0. \quad (18)$$

We note that the essentially non-geostrophic terms for the vertical vorticity advection, the twisting effect, and the non-linear divergence term have been neglected (as in (4)), and also that the vorticity advection by the divergent wind is ignored. The generalization of (18) relative to the quasi-geostrophic case is thus principally in the retention of the divergence term without restriction of the Coriolis parameter. As shown by Lorenz (1960), the form of the balance equation consistent with (18) is

$$\nabla^2\phi - \nabla\cdot(f\nabla\psi) = 0, \quad (19)$$

in which the Coriolis parameter is again not restricted. The adiabatic, continuity, and hydrostatic equations accompanying (18) and (19) are

$$\frac{\partial\theta}{\partial t} + J(\psi, \theta) + \nabla\chi\cdot\nabla\theta + \omega\frac{\partial\theta}{\partial p} = 0, \quad (20)$$

$$\frac{\partial\omega}{\partial p} + \nabla^2\chi = 0, \quad (21)$$

$$\frac{\partial\phi}{\partial p} + \frac{RT}{p} = 0. \quad (22)$$

In (20), we may note, the temperature advection by the divergent wind is included, an effect not present in the quasi-geostrophic case (6). It is also important to note in this connection that the static stability $\partial\theta/\partial p$ in (20) is not restricted.

Again dividing the atmosphere into four equal layers of $p_0/4$, applying (18), (20) and (21) at the upper and lower interior levels 1 and 3, and using centered finite differences to evaluate the (first) pressure derivative of ϕ, ω and θ, we find the system

$$\nabla^2\left(\frac{\partial\psi}{\partial t}\right) + J(\psi, \nabla^2\psi + f) + J(\tau, \nabla^2\tau) = 0, \quad (23)$$

$$\nabla^2\left(\frac{\partial\tau}{\partial t}\right) + J(\tau, \nabla^2\psi + f) + J(\psi, \nabla^2\tau) - \nabla\cdot(f\nabla\chi) = 0), \quad (24)$$

$$\nabla^2\omega + \frac{1}{\sigma}\left(\nabla^2\sigma - f^2R^{-1}2^{\varkappa+1}\right)\omega$$

$$= \frac{p_0}{2\sigma}[\nabla^2J(\psi,\theta) + \nabla^2J(\tau,\sigma)] - \frac{2^\varkappa p_0 f}{R\sigma}$$

$$\times [J(\tau, \nabla^2\psi + f) + J(\psi, \nabla^2\tau)]$$

$$+ \frac{1}{\sigma}\left[\frac{2^\varkappa p_0}{R}\nabla f\cdot\nabla\frac{\partial\tau}{\partial t} + \frac{2^\varkappa p_0 f}{R}\nabla f\cdot\nabla\chi\right.$$

$$\left. - \frac{p_0}{2}\nabla^2(\nabla\sigma\cdot\nabla\chi) - 2\nabla\sigma\cdot\nabla\omega\right], \quad (25)$$

$$\frac{\partial\sigma}{\partial t} + J(\psi,\sigma) + J(\tau,\theta) - \nabla\theta\cdot\nabla\chi = 0, \quad (26)$$

$$\nabla^2\theta = \frac{2^{\varkappa+1}}{R}(\nabla f\cdot\nabla\tau + f\nabla^2\tau), \quad (27)$$

$$\nabla^2\chi = \frac{2\omega}{p_0}. \quad (28)$$

Here the new dependent variables are defined as

$$\psi = (\psi_1 + \psi_3)/2, \quad (29)$$

$$\tau = (\psi_1 - \psi_3)/2, \quad (30)$$

$$\theta = (\theta_1 + \theta_3)/2, \quad (31)$$

$$\sigma = (\theta_1 - \theta_3)/2, \quad (32)$$

$$\chi = (\chi_3 - \chi_1)/2, \quad (33)$$

$$\omega = \omega_2. \quad (34)$$

Equations (23) and (24), representing this model's mean and thermal vorticity equations, are similar in form to (9) and (10) for the usual two-level model. Equation (25) for the vertical motion ω resembles (11) for the conventional model, but is complicated by terms representing the spatial variation of both the static stability σ and the Coriolis parameter f. Equation (26) for the static stability variation is, of course, not present in the model with a constrained (constant) stability; here (26) results from the application of the adiabatic equation at the *two* levels 1 and 3, while in the usual quasi-geostrophic model this application is made only at the central level 2. We also note that (27), a form of the thermal wind relation, permits full variation of f. In connection with the present numerical solutions of the balanced variable–stability model, it will prove necessary, however, to restrict slightly the spatial variations of σ and f, as will be discussed in a later section.

5. The finite-difference grid and general solution method

In order to minimize boundary condition errors and at the same time to examine the largest scales of motion, the numerical integrations were carried out on a finite-difference grid covering the entire northern hemisphere. This grid consists of the net of points extending over the earth's spherical surface spaced every 5 degrees latitude and 5 degrees longitude, with the pole itself treated separately. Ordinary centered differences are generally employed on this grid, with some points skipped in the longitudinal direction at the higher latitudes in order to maintain comparable resolution over the sphere. Viewing this grid as an array of 72×18 points (plus one point at the pole), and denoting the eastward and northward grid directions by the integer indices i and j, respectively, we may say that latitudinal differentials are evaluated by reference to the points $j \pm 1$ and longitudinal differentials by reference to the points $i \pm m$. At latitudes $\varphi \leq 70$ N, $m = 1$, i.e., the neighboring points are used in a (first) derivative estimate, $m = 2$ at $\varphi = 75$ N, $m = 3$ at 80 N, and $m = 6$ at $\varphi = 85$ N. This set of points is shown in Fig. 1. This grid has previously been successfully used in the integration of the barotropic model, and further details of its design have been given elsewhere (GATES & RIEGEL, 1962*a*, 1962*b*).

In order to insure uniform computational procedures, a number of library or standard subroutines were written for the evaluation of the operators common to the models' governing equations. Let us first denote the earth's assumed spherical radius by r, the latitudinal mesh spacing by $\Delta\varphi$, and the longitudinal mesh spacing by $m\Delta\lambda$, with $m = 1$, 2, 3 or 6 as described above for $\Delta\varphi = \Delta\lambda = 5$ deg. Let us also introduce the dimensionless ratios

$$n_1 = \frac{m\Delta\lambda}{\Delta\varphi}\cos\varphi, \quad (35)$$

$$n_2 = \frac{m\Delta\lambda}{2}\sin\varphi. \tag{36}$$

If a is an arbitrary scalar variable, the Laplacian operator $\nabla^2 a$ was approximated by

$$\nabla^2 a_{ij} = n_1^{-1}(r\Delta\varphi)^{-2}[(n_1 - n_2)a_{ij+1} + (n_1 + n_2)a_{ij-1} + n_1^{-1}(a_{i+mj} + a_{i-mj}) - (2n_1 + 2n_1^{-1})a_{ij}] \tag{37}$$

for non-polar points, and by

$$\nabla^2 a_p = (2/3)(r\Delta\varphi)^{-2}(a_1 + a_2 + a_3 + a_4 + a_5 + a_6 - 6a_p) \tag{38}$$

at the pole itself, denoted by the subscript p. In (38) the subscripts 1–6 denote six equally spaced points at 85 N on a local polar hexagonal grid, from which the form of (38) itself was determined.

If a and b are two arbitrary scalar variables, the Jacobian operator $J(a, b)$ was approximated at non-polar points by

$$J(a, b)_{ij} = (4n_1)^{-1}(r\Delta\varphi)^{-2}[(a_{i+mj} - a_{i-mj}) \times (b_{ij+1} - b_{ij-1}) - (a_{ij+1} - a_{ij-1}) \times (b_{i+mj} - b_{i-mj})], \tag{39}$$

and at the pole by

$$J(a,b)_p = (6\sqrt{3})^{-1}(r\Delta\varphi)^{-2} \times [(b_1 - b_4)(a_5 + a_6 - a_2 - a_3) + (b_2 - b_5)(a_1 + a_6 - a_3 - a_4) + (b_3 - b_6)(a_1 + a_2 - a_4 - a_5)]. \tag{40}$$

The operators $\nabla a \cdot \nabla b$ and $\nabla \cdot (a\nabla b)$ were approximated in a similar fashion.

With the non-homogeneous terms of the model's governing equations evaluated, the solution for tendencies or for ω was made by the extrapolated Liebmann relaxation method. This consisted of first calculating the residues R_{ij} relative to an initial guess for, say $(\partial\psi/\partial t)_{ij}$, and systematically modifying the solution according to

$$\left(\frac{\partial\psi}{\partial t}\right)^1_{ij} = \left(\frac{\partial\psi}{\partial t}\right)^0_{ij} + \alpha R_{ij}, \tag{41}$$

where α is the over-relaxation coefficient. The relaxation continued until

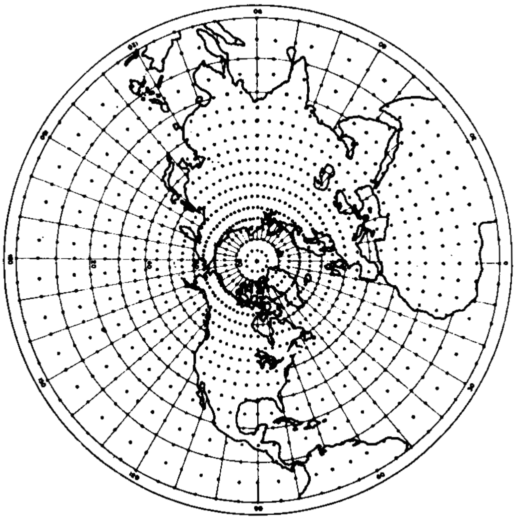

FIG. 1. The hemispheric grid-point network used for the construction of finite-difference estimates in the numerical integrations.

$$|R_{ij}| \leqslant \varepsilon, \tag{42}$$

for all ij. The appropriate values of α and ε have been determined experimentally for each model equation. Upon completion of the relaxation, the time extrapolation is carried out by the usual centered finite-difference in time, with the initial step using a forward difference. Further details of the solution procedure will be discussed below in connection with the individual models; reference may also be made to GATES & RIEGEL (1962*a*, 1962*b*).

6. The test data

It was desired to select a case whose subsequent development showed well-documented cyclogenesis and which at the same time contained typical large-scale disturbances at various stages of their life-cycle. The greatest possible upper-air coverage over the northern hemisphere was also desired. These conditions were met satisfactorily by the case of 00 GCT, 7 December 1957, at which time the observational program of the International Geophysical Year was in progress. This case presents a number of open propagating long waves around the hemisphere, an amplifying system over the United States, and a weak blocking pattern over the eastern Atlantic. The contour, tem-

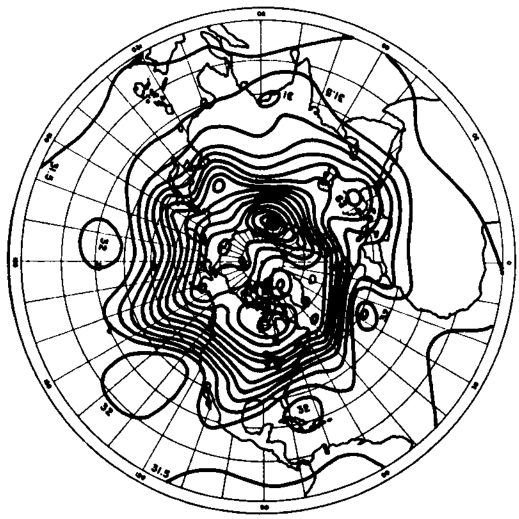

FIG. 2a. The initial contours at 700 mb on 00 GCT, 7 December 1957. The contours are drawn each 50 m, and the labels are in 10^2 m.

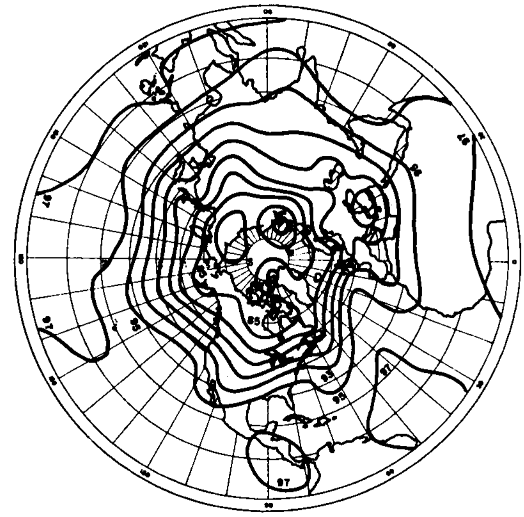

FIG. 3a. The initial contours at 300 mb on 00 GCT, 7 December 1957. The contours are drawn each 200 m and are labeled in 10^2 m.

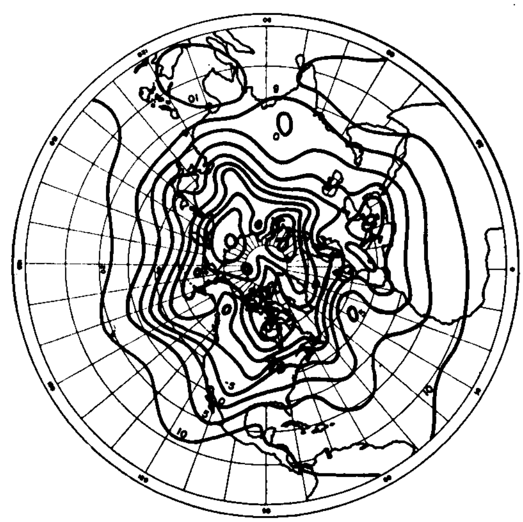

FIG. 2b. The initial isotherms at 700 mb on 00 GCT, 7 December 1957. The isotherms are drawn each 5 deg and are labeled in deg C.

FIG. 3b. The initial isotherms at 300 mb on 00 GCT, 7 December 1957. The isotherms are drawn each 5 deg and are labeled in deg C.

perature, and wind data for this case was read from IGY microcards, plotted, and analyzed for the 700 mb and 300 mb surfaces, and are shown in Figs. 2 and 3. These data formed the basis of the initial conditions for each of the three test models. The later 00 GCT maps for 8, 9, and 10 December 1957 were also used for the construction of verification maps in terms of the specific variables of each model.

7. The numerical solution of the barotropic model

The numerical solution of (1) was found from the approximating difference equation

$$\nabla^2\left(\frac{\partial\psi}{\partial t}\right)_{ij} = -J(\psi, \nabla^2\psi + f)_{ij}, \qquad (43)$$

where the difference operators are given by

FIG. 4. The initial ($t = 0$) distribution of the streamfunction ψ, obtained from (44) with $\psi = 0$ at the equator. The labeled units are 10^7 m^2 sec^{-1}.

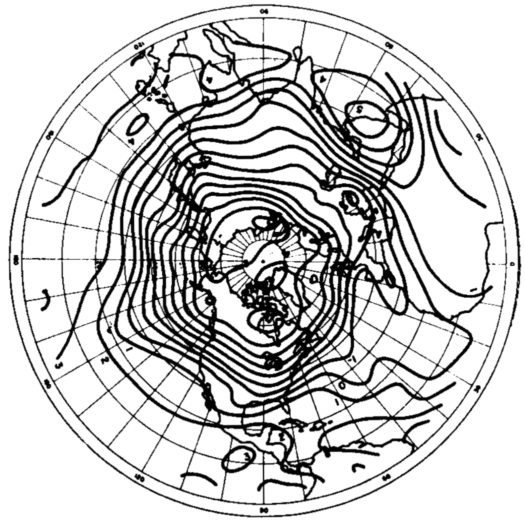

FIG. 5. The forecast distribution of the streamfunction ψ from the barotropic model, for 00 GCT, 8 December 1957 ($t = 24$ hr). The units are 10^7 m^2 sec^{-1}.

(37)–(40). Accompanying (43) is the difference analogue of (3),

$$\nabla \cdot (f \nabla \psi)_{ij} = \nabla^2 \phi_{ij}. \qquad (44)$$

The value of ϕ (geopotential) here was taken at all points as

$$\phi = g(z_{300} + z_{700})/2,$$

where g is the gravitational acceleration, and z_{300} and z_{700} are the 300 mb and 700 mb contour heights from the initial data. With a boundary condition $\psi = 0$ at the equator, (44) was solved by relaxation according to (41) and (42), with the values $\alpha = 0.21$ and $\varepsilon = 0.3 \times 10^4$ m^2 sec^{-1}, and required 519 scans for convergence. This solution was aided by the use of block relaxation within successive latitude circles after every 20th scan. The ψ solution is shown in Fig. 4, and bears a close resemblance to the initial 500 mb contour map.

With ψ now determined (at $t = 0$), the solution of (43) was obtained by relaxation with $\varepsilon = 0.05$ m^2 sec^{-2} and $\alpha = 0.302$, for the boundary condition $\partial\psi/\partial t = 0$ at 5 N; thus the values of ψ found at 5 N from (44) from the observed ϕ field were held constant in time. The condition $\psi = 0$ at the equator is also present, but is not directly involved in the solution of (43) at a given time. The numerical solution for ψ at $t = 24$ hr is shown in Fig. 5, made with a conventional centered time step $\Delta t = 1/2$ hr (with a forward step at $t = 0$). The corresponding observed or verification ψ field found from (44) from the observed contour distributions is shown in Fig. 6. We may note the eastward movement of the trough over the northern United States and the lagging pattern in the southwestern United States. This distortion of an open wave is typical of the non-divergent

FIG. 6. The observed distribution of the streamfunction ψ at 00 GCT, 8 December 1957 ($t = 24$ hr), in units of 10^7 m^2 sec^{-1}.

barotropic model and is associated with this model's persistent northward transport of westerly momentum. The effect of the smaller longitudinal grid spacing in the north is not believed to be significant at these latitudes, although it acts in the sense of creating such an effect (GATES & RIEGEL, 1962b). The intensification of this wave over the United States was not correctly forecast and evidently represents a baroclinic development. Over the Pacific Ocean and Asia, the wave systems' movements were forecast with reasonable accuracy, and the nearly stationary systems over Europe were successfully retained.

The 48 and 72 hr forecasts show further distortion of the shape and amplitude of the wave over the eastern United States. Over the eastern Pacific, Europe and Africa, there are now relatively serious errors of amplitude, shape and position. Such forecasts are undoubtedly inferior to those which would be produced by the operational barotropic model of the National Meteorological Center (CRESSMAN, 1960), with its long-wave controls and smoothing; these effects were deliberately withheld from the present formulation.

8. The numerical solution of the 2-level quasi-geostrophic model

The numerical solution of the system (9)–(12) was found from the approximating difference system

$$\nabla^2\left(\frac{\partial\psi}{\partial t}\right)_{ij} + J(\psi, \nabla^2\psi + f)_{ij} + J(\tau, \nabla^2\tau)_{ij} = 0, \quad (45)$$

$$\nabla^2\left(\frac{\partial\tau}{\partial t}\right)_{ij} + J(\tau, \nabla^2\psi + f)_{ij} + J(\psi, \nabla^2\tau)_{ij} - \frac{2f_0}{p_0}\omega_{ij} = 0, \quad (46)$$

$$\sigma_0\nabla^2\omega_{ij} - 2^{\varkappa} f_0^2 R^{-1}\omega_{ij} = \frac{p_0}{4}\nabla^2 J(\psi, \theta)_{ij} - \frac{2^{\varkappa-1} f_0 p_0}{R}[J(\tau, \nabla^2\psi + f)_{ij} + J(\psi, \nabla^2\tau)_{ij}], \quad (47)$$

$$\theta_{ij} = 2^{\varkappa+1} f_0 R^{-1}\tau_{ij} \quad (48)$$

Starting from the initial contour data at 300 mb and 700 mb, the variables ψ and τ were determined at all latitudes from $\psi, \tau = g(z_{300} \pm z_{700})/2f_0$. The static stability σ_0 in (47) was determined from the relation

$$\sigma_0 = (5/4)(\bar\theta_{300} - \bar\theta_{700})/2 = 16.5 \text{ deg},$$

where $\bar\theta_{300}$ and $\bar\theta_{700}$ are the hemispheric average potential temperatures at 300 mb and 700 mb, respectively, as determined by analysis of the temperature initial data in the test case.[1] With ψ, τ and θ determined (at $t=0$), the solution for ω_{ij} was next obtained, followed by the solutions for $\partial\tau/\partial t$ and $\partial\psi/\partial t$.

In the relaxation solution for ω_{ij}, the constants $\alpha = 0.215$ and $\varepsilon = 0.01$ mb hr^{-1} were used, with the boundary condition $\omega = 0$ at 5 N ($\omega = 0$ also at the equator when needed). In the solution for $(\partial\tau/\partial t)_{ij}$ the values $\alpha = 0.260$ for $\varepsilon = 0.5$ m^2 sec^{-2} was selected, with the boundary condition $\partial\tau/\partial t = 0$ at 5 N. At the equator, τ was set equal to the equatorial average of the initially determined $\tau(\lambda)$ and held fixed. Finally, in the solution for $(\partial\psi/\partial t)_{ij}$ values $\alpha = 0.290$, and $\varepsilon = 0.5$ m^2 sec^{-2} were selected, with boundary conditions at ON and 5 N analogous to those for τ.

The distribution of ψ at $t=0$ for the test case (OO GCT, 7 December 1957) closely resembles that for the barotropic model (Fig. 4). The initial τ (or θ) field is shown in Fig. 7, and is seen to be nearly coincident with the mean streamfunction (ψ) field, in testimony to the atmosphere's overall quasi-barotropy. Over the United States and the central Pacific, however, the thermal field lags westward relative to the ψ field, and the subsequent development of these two systems (while the hemisphere's remaining systems show little change) supports this configuration as an index of baroclinic development. Whether or not the model itself will *predict* this development is, of course, another question. The distribution of ω at $t=0$ accompanying Fig. 7 is shown in Fig. 8. Here we see a pattern of rising motion ($\omega < 0$) to the east of nearly every ψ trough, with sinking motion ($\omega > 0$) to the west. These fields of ω are characteristically curved westward toward lower latitude, paralleling the familiar configuration of the mid-latitude system. The maximum middle-latitude ω is here 12 mb hr^{-1}.

[1] The coefficient 5/4 arises from the ratio (750 mb–250 mb)/(700 mb–300 mb), taking 750–250 mb as the standard depth for measurement of stability here as in the two-layer model of variable stability (see (32)).

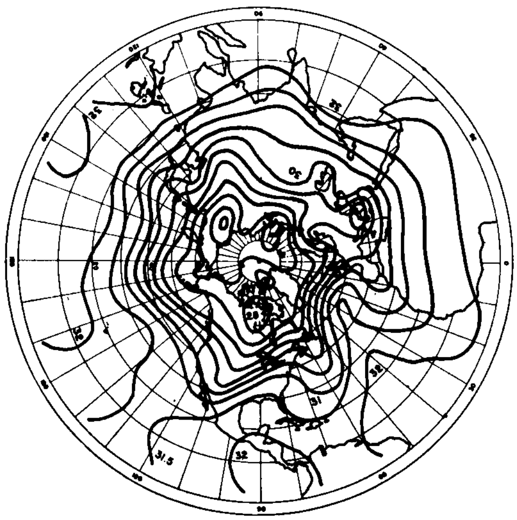

FIG. 7. The initial ($t=0$) distribution at 00 GCT, 7 December 1957 of the streamfunction τ, obtained with the quasi-geostrophic two-level model with $\tau = 320 \times 10^6$ m^2 sec^{-1} at the equator. The units are 10^7 m^2 sec^{-1}. The distribution of the temperature θ is proportional to τ through (48).

The numerical integrations of the two-level quasi-geostrophic model (45)–(48) have given the distributions of ψ, τ and ω at $t = 24$ hr shown in Figs. 9, 11 and 13, while Figs. 10, 12, and 14 show the corresponding verification or "observed" distributions. The ψ field (Figs. 9 and 10) is forecast to move generally eastward, much in the manner of the barotropic model (Figs. 5 and 6). The τ field (Figs. 11 and 12) is moved too rapidly eastward over the United States, and the southwestern tilt characteristic of the ψ field has also been forecast for τ. Over the United States in particular, this error has

FIG. 8. The initial ($t=0$) distribution at 00 GCT, 7 December 1957 of the vertical motion ω, obtained with the quasi-geostrophic two-level model (47) with $\omega = 0$ at 5 N. The units are mb hr^{-1}. The isolines -5, -1, 3, 7, ... are drawn, with the area of ω more negative than -1 shaded.

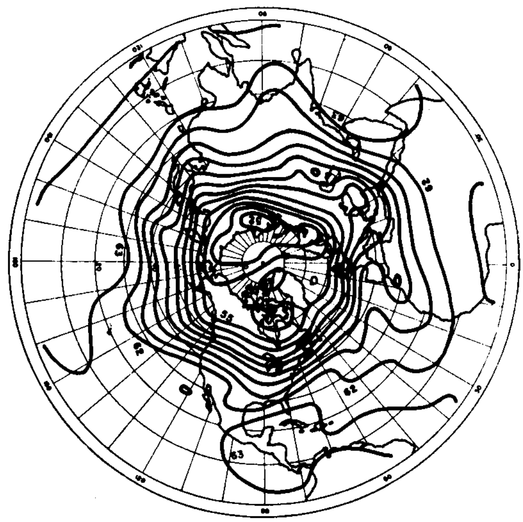

FIG. 9. The forecast distribution of the streamfunction ψ from the two-level quasi-geostrophic model, for 00 GCT, 8 December 1957 ($t = 24$ hr). The units are 10^7 m^2 sec^{-1}.

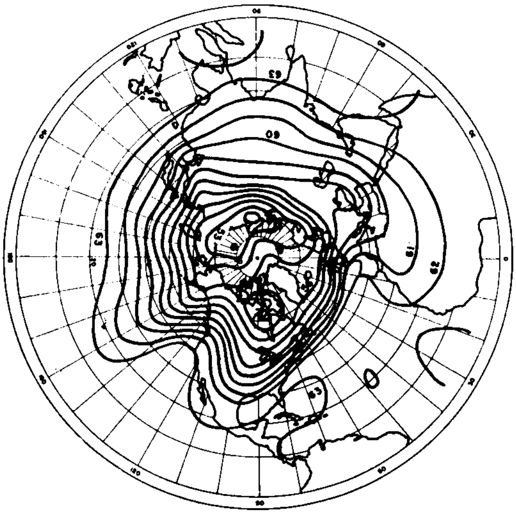

FIG. 10. The observed distribution of the streamfunction ψ from the two-level quasi-geostrophic model for 00 GCT, 8 December 1957. The units are 10^7 m^2 sec^{-1}.

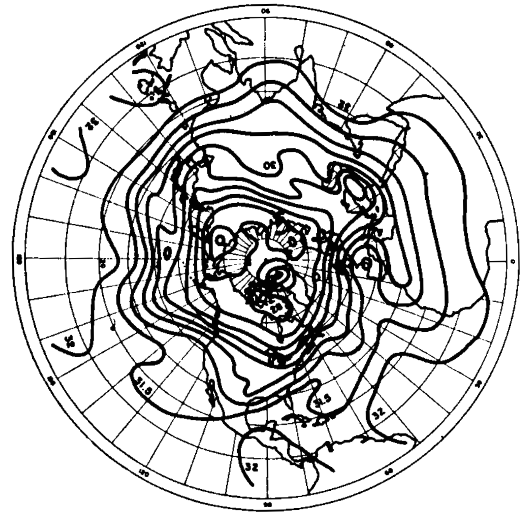

FIG. 11. The forecast distribution of the streamfunction τ from the two-level quasi-geostrophic model, for 00 GCT, 8 December 1957 ($t = 24$ hr). The units are 10^7 m^2 sec^{-1}.

FIG. 13. The forecast distribution of the vertical motion ω from the two-level quasi-geostrophic model, for 00 GCT, 8 December 1957 ($t = 24$ hr). The units are mb hr^{-1}. See Fig. 8.

resulted in a notably poor forecast of the τ field, and it is evident that the model has here failed to predict the thermal trough amplification and the accompanying development of the system. The ω distributions in Figs. 13 and 14 show a fair degree of correspondence, with the maximum forecast ω now 13 mb hr^{-1}.

In the integrations to 48 and 72 hr the ψ field continues to be similar to the barotropic model, with the deepening of the system over the United States continuing to escape the model. The τ field forecast now shows generally damped long waves and a number of cut-off pools of cold and warm air in the latitudes

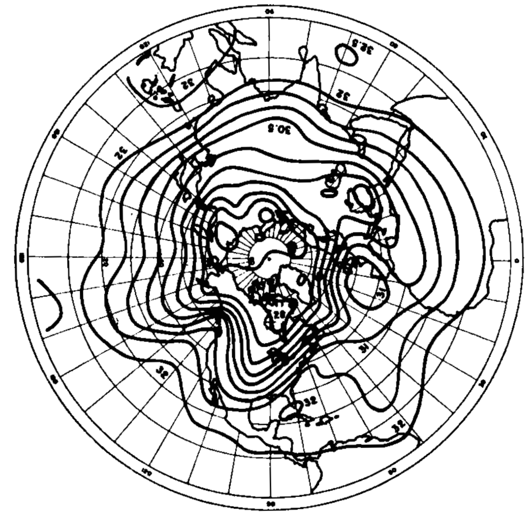

FIG. 12. The observed distribution of the streamfunction τ from the two-level quasi-geostrophic model for 00 GCT, 8 December 1957. The units are 10^7 m^2 sec^{-1}.

FIG. 14. The observed distribution of the vertical motion ω from the two-level quasi-geostrophic model for 00 GCT, 8 December 1957. The units are mb hr^{-1}. See Fig. 8.

30–40 N, in contrast to the "observed" τ distribution. The ω forecast is now rather cellular and distorted, although the magnitudes of ω do not appear excessive. During the course of the 72 hr integration, the forecast meridional zonal wind profile shows a continued increase of the high- and low-latitude easterlies, and an increase of the westerlies between approximately 35 N and 50 N. This clearly demonstrates the mid-latitude convergence of westerly momentum, and may be regarded as an essentially barotropic process. The mean meridional circulation given by the forecast profiles of the zonal average ω remains the familiar three-cell structure with the thermally direct cells of high and low latitudes becoming relatively too strong in the forecast.

9. The numerical solution of the two-layer balanced model of variable static stability

The numerical solution of the system (23)–(28) was found from the approximating difference equations

$$\nabla^2\left(\frac{\partial\psi}{\partial t}\right)_{ij} + J(\psi, \nabla^2\psi+f)_{ij} + J(\tau, \nabla^2\tau)_{ij} = 0, \quad (49)$$

$$\nabla^2\left(\frac{\partial\tau}{\partial t}\right)_{ij} + J(\tau, \nabla^2\psi+f)_{ij} + J(\psi, \nabla^2\tau)_{ij} - \nabla\cdot(f\nabla\chi)_{ij} = 0 \quad (50)$$

$$\begin{aligned}\nabla^2\omega_{ij} &+ \frac{1}{\sigma_{ij}}(\nabla^2\sigma_{ij} - f^2 2^{\varkappa+1}R^{-1})\,\omega_{ij}\\ &= \frac{p_0}{2\sigma_{ij}}[\nabla^2 J(\psi,\theta)_{ij} + \nabla^2 J(\tau,\sigma)_{ij}] - \frac{2^{\varkappa}p_0 f}{R\sigma_{ij}}\\ &\quad\times[J(\tau, \nabla^2\psi+f)_{ij} + J(\psi, \nabla^2\tau)_{ij}]\\ &\quad+\frac{2^{\varkappa}p_0\nabla f\cdot\nabla\left(\frac{\partial\tau}{\partial t}\right)_{ij}}{R\sigma_{ij}} + \frac{1}{\sigma_{ij}}\left\{\frac{2^{\varkappa}p_0 f}{R}\nabla f\cdot\nabla\chi_{ij}\right.\\ &\quad\left.-\frac{p_0}{2}\nabla^2(\nabla\sigma\cdot\nabla\chi)_{ij} - 2\nabla\sigma\cdot\nabla\omega_{ij}\right\},\end{aligned} \quad (51)$$

$$\left(\frac{\partial\sigma}{\partial t}\right)_{ij} + J(\psi,\sigma)_{ij} + J(\tau,\theta)_{ij} - \nabla\theta\cdot\nabla\chi_{ij} = 0, \quad (52)$$

$$\nabla^2\theta_{ij} = \frac{2^{\varkappa+1}}{R}(\nabla f\cdot\nabla\tau_{ij} + f\nabla^2\tau_{ij}), \quad (53)$$

$$\nabla^2\chi_{ij} = \frac{2}{p_0}\omega_{ij}. \quad (54)$$

In comparison to (47) for the two-level quasi-geostrophic model, the solution of (25) as (51) presents some particular difficulties. First, the permitted variation of the Coriolis parameter f may lead to a violation of the conservation of mass, in spite of the energetically consistent formulation of the model. If we integrate (25) over the total mass of the atmosphere ($dm = g^{-1}dx\,dy\,dp$), and use the continuity equation (28) in the term $2^{\varkappa}p_0 fR^{-1}\nabla f\cdot\nabla\chi$, we find

$$\int f^2\omega\,dm = p_0\int f[J(\tau, \nabla^2\psi+f) + J(\psi, \nabla^2\tau)]\,dm - p_0\int\nabla f\cdot\nabla\frac{\partial\tau}{\partial t}\,dm. \quad (55)$$

However, the continuity equation itself requires $\int\omega\,dm = 0$ and this property can be ensured from the ω-equation's solution only when f and $|\nabla f| = \beta$ are taken as constants in the terms of (55). Hence we have written (51) in the form

$$\begin{aligned}\nabla^2\omega &+ \frac{1}{\sigma_{ij}}(\nabla^2\sigma_{ij} - f_0^2 2^{k+1}R^{-1})\,\omega_{ij}\\ &= \frac{p_0}{2\sigma_{ij}}[\nabla^2 J(\psi,\theta)_{ij} + \nabla^2 J(\tau,\sigma)_{ij}] - \frac{2^{\varkappa}p_0 f_0}{R\sigma_{ij}}\\ &\quad\times[J(\tau, \nabla^2\psi+f)_{ij} + J(\psi, \nabla^2\tau)_{ij}]\\ &\quad+\frac{2^{\varkappa-1}p_0\beta_0}{\sigma_{ij}Rr\Delta\varphi}\left(\left(\frac{\partial\tau}{\partial t}\right)_{j+1} - \left(\frac{\partial\tau}{\partial t}\right)_{j-1}\right)\\ &\quad+\frac{1}{\sigma_{ij}}\left\{\frac{2^{\varkappa}p_0 f}{R}\nabla f\cdot\nabla\chi_{ij} - \frac{p_0}{2}\nabla^2(\nabla\sigma\cdot\nabla\chi)_{ij}\right.\\ &\quad\left.- 2\nabla\sigma\cdot\nabla\omega_{ij}\right\}.\end{aligned} \quad (56)$$

We note that these restrictions of f are selective, and that they occur *only* in the present ω-equation.

A second consideration in the solution of (51) arises from the permitted variability of the static stability σ and the Coriolis parameter f which makes the coefficient of the ω_{ij}-term on the left-hand side of (25) or (51) a variable quantity, and one which may, moreover, change sign. To consider this effect, let us write (25) in the form

$$\nabla^2\omega + \mu F(x,y,t)\,\omega = G(x,y,t), \qquad (57)$$

where G denotes the right-hand side of (25) and where

$$\mu F(x,y,t) = \frac{1}{\sigma}(\nabla^2\sigma - f^2 2^{\varkappa+1}R^{-1}). \qquad (58)$$

According to SOMMERFELD (1949), the homogeneous equation corresponding to the above,

$$\nabla^2\omega + \lambda F(x,y,t)\,\omega = 0, \quad F > 0, \qquad (59)$$

possesses a solution with the boundary condition $\omega = 0$ only when $F > 0$. In the non-homogeneous case, therefore, we must assume that no μ equals an eigen value λ, and that $F(x,y,t) > 0$ for arbitrary $G(x,y,t)$. Hence, $\mu F(x,y,t)$ must have the same sign everywhere if the (non-homogeneous) ω equation is to have a solution. Assuming that this argument also applies in the difference case (56), we thus require that $(\nabla^2\sigma_{ij} - f_0^2 2^{\varkappa+1}R^{-1})$ does not change sign. Since $f_0^2 2^{\varkappa+1}R^{-1} > 0$ and since $\nabla^2\sigma_{ij}$ characteristically changes sign in large-scale flow, we introduce the restriction

$$\nabla^2\sigma_{ij} < f_0^2 2^{\varkappa+1}R^{-1} \qquad (60)$$

for all points at and beyond 10 N. At points where this restriction is violated by the existing σ_{ij} field, $\nabla^2\sigma_{ij}$ is arbitrarily assigned the value $0.75 f_0^2 2^{\varkappa+1}R^{-1}$. Equation (56) now replaces (51), and the values $f_0 = 1.37 \times 10^{-4}$ sec^{-1} and $\beta_0 = 7.83 \times 10^{-12}$ m^{-1} sec^{-1} appropriate to 70 N were selected for use with the restriction (60).

Starting from the initially observed contour z and temperature T fields at 300 mb and 700 mb, the corresponding initial distributions of the variables ψ and τ were determined from the relations $f\nabla^2(\psi,\tau) + \beta\partial(\psi,\tau)/\partial y = g\nabla^2(z_{300} \pm z_{700})/2$, and $\sigma = 5(\theta_{300} - \theta_{700})/8$. These ψ and τ relaxations used the values $\alpha = 0.21$ and $\varepsilon = 0.3 \times 10^4$ m^2 sec^{-1}, with the equatorial boundary conditions $\psi, \tau = \frac{1}{2} g f_0^{-1}(\bar{z}_{300} \pm \bar{z}_{700})$, where $f_0 = 10^{-4}$ sec^{-1} and the bar ($^-$) denotes a longitudinal average (at ON). With ψ, τ, and σ determined (at $t = 0$), the solution of the system (49, 50, 52–54, 56) was obtained in the following sequence: (i) θ_{ij} is determined from (53) by relaxation; (ii) $(\partial\tau/\partial t)_{ij}$ is found from (50) (in the initial use of this step, the last right-hand term is zero); (iii) ω_{ij} is found from (56) by relaxation (in the initial use of this step the terms within the brace $\{\ \}$ are zero); (iv) χ_{ij} is found from (54) by relaxation, using the ω_{ij} from the previous step; (v) $(\partial\tau/\partial t)_{ij}$ is redetermined from (56), now using the entire right-hand side with the above-determined values of χ_{ij} and ω_{ij}. Steps (ii)–(iv) are now repeated, using the latest available $\partial\tau/\partial t$, χ, and ω, until successive solutions for ω_{ij} satisfy $|\omega_{ij}^{n+1} - \omega_{ij}^{n}| \leq \varepsilon^* = 0.1$ mb hr^{-1}. At this point steps (iv) and (ii) are repeated once more to yield values of $(\partial\tau/\partial t)_{ij}$ and χ_{ij} corresponding to the convergent ω_{ij} just found. Then, finally, (vi) $(\partial\sigma/\partial t)_{ij}$ is determined from (52), and (vii) $(\partial\psi/\partial t)_{ij}$ is found from (49). From the tendency solutions, values of ψ, τ and σ are constructed at $t = \Delta t$ ($= 1/2$ hr) by use of an initially forward time step, after which the above sequence (i)–(vii) is repeated. At subsequent iterations, the conventional centered time step is used. In these relaxations, the following boundary conditions at 5 N were used: $\partial\psi/\partial t = 0$, $\partial\tau/\partial t = 0$, $\omega = 0$, and $\chi = 0$. In addition at ON, $\sigma = \sigma(\lambda)$ as initially determined, and $\theta = \bar{\theta}$, the average of the initial equatorial values.

At $t = 0$ a number of trial relaxations were made with various values of the over-relaxation coefficient α and of the residue tolerance ε, from which the optimum values were determined. These data are summarized in Table 1. In general the number of scans required at $t = 0$ was somewhat higher than those shown (with zero initial guess). Although the scans tended generally to increase with the forecast length, those for the ω_{ij} and χ_{ij} solutions in particular showed a marked increase beyond

TABLE 1. *Data for the relaxation solution (41)–(42) of the two-layer model of variable stability.*

Variable (eq.)	Selected ε	Optimum α	No. of scans per time step[b]
θ (53)	0.1 deg	0.18[a]	12–40
$\partial\tau/\partial t$ (50)	0.5 m^2 sec^{-2}	0.28	100
ω (56)	0.0075 mb hr^{-1}	0.16	59–110
χ (54)	0.5 × 10^4 m^2 sec^{-1}	0.20[a]	40–150
$\partial\psi/\partial t$ (49)	0.5 m^2 sec^{-2}	0.29	50–70

[a] Block relaxation performed every 5 scans.
[b] In 24 hr forecast.

FIG. 15. The initial ($t = 0$) distribution at 00 GCT, 7 December 1957 of the stability σ, obtained with the two-layer variable stability model. The units are deg.

FIG. 16. The initial ($t = 0$) distribution at 00 GCT, 7 December 1957 of the vertical motion ω, obtained with two-layer variable stability model from (56). The units are mb hr^{-1}. The isolines -7, -1, 5, ... are drawn, with the area of ω more negative than -1 shaded.

24 hr. In step (v), the redetermination of ω_{ij}, from 3 to 7 successive approximations were required, with the same number of successive approximations for $(\partial\tau/\partial t)_{ij}$ and χ_{ij} also needed.

The initial distributions of ψ and τ closely resemble those of the usual two-level quasi-geostrophic model (see Figs. 4 and 7); the distribution of θ closely resembles that of τ. The initial σ field (given in Fig. 15) shows a synoptic-scale pattern, with the relatively stable air frequently east of troughs and the relatively unstable air to the west. The actual values of σ here range from 9 to 25 degrees. In meridional profile, the lowest σ is present in the middle-latitudes 25 N–55 N.

The solution of (56) for ω_{ij} is shown in Fig. 16, and displays a synoptic pattern similar to that of the ω_{ij} determined from the quasi-geostrophic two-level model (Fig. 8), except that in the present case the magnitude of ω_{ij} is approximately twice as great. This effect is basically due to the application of the adiabatic equation at *two* levels in the two-layer balanced model, rather than at only a single level as in the quasi-geostrophic case (GATES, 1961). With the present σ distribution, the relatively stable air is here often rising ($\omega < 0$) and the relatively unstable air sinking ($\omega > 0$); if this correlation persists in time, it would tend to prevent the occurrence of extreme values of σ, and hence may represent a self-control mechanism of the model. The meridional profile of the zonal average $\bar{\omega}$ ($t = 0$), shown in Fig. 17, suggests a slightly stronger three-cell meridional circulation in comparison with that of the usual two-level quasi-geostrophic model, and in general the present ω_{ij} is felt to be superior as a diagnostic calculation. The initial χ_{ij} distribution accompanying this ω_{ij} shows convergence ahead (east) of a trough and divergence behind, corresponding to the expected lower level divergence pattern ($\chi = \chi_3$ here). The maximum magnitude of the divergent wind speed is about 4 m sec^{-1}, or about 10 % of the maximum non-divergent wind speed estimated from ψ.

The 24 hr forecast distribution of ψ from the two-layer balanced model is shown in Fig. 18. This forecast generally resembles those made with the barotropic and quasi-geostrophic two-level models (Figs. 5 and 9), and it is immediately evident that the two-layer balanced baroclinic model, like its quasi-geostrophic counterpart, has failed to predict the baroclinic development of the major systems over the eastern-north Pacific and, more spectacularly, over the eastern United States (see Fig. 10). In meridional profile, the present model has an identical initial zonal wind with the barotropic

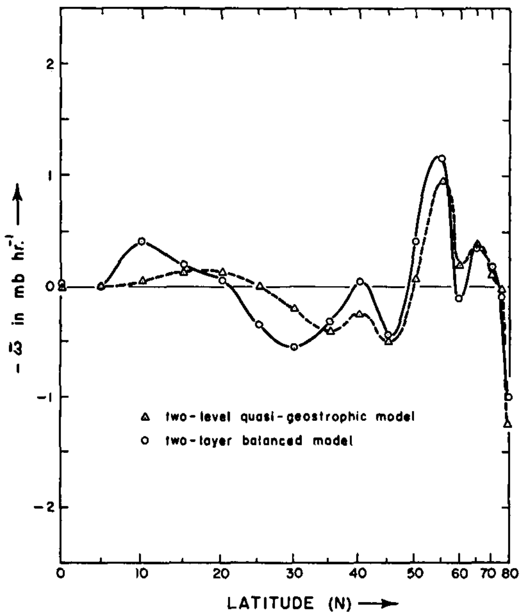

FIG. 17. The merdiional profile of the zonal average vertical motion $\bar{\omega}$, determined at $t=0$ (00 GCT, 7 December 1957) from the two-level quasi-geostrophic model (47) and from the two-layer balanced (variable stability) model (56).

model, but by 24 hr it has surpassed even this model's erroneous increase of middle-latitude westerlies.

The forecast fields of τ and θ resemble those

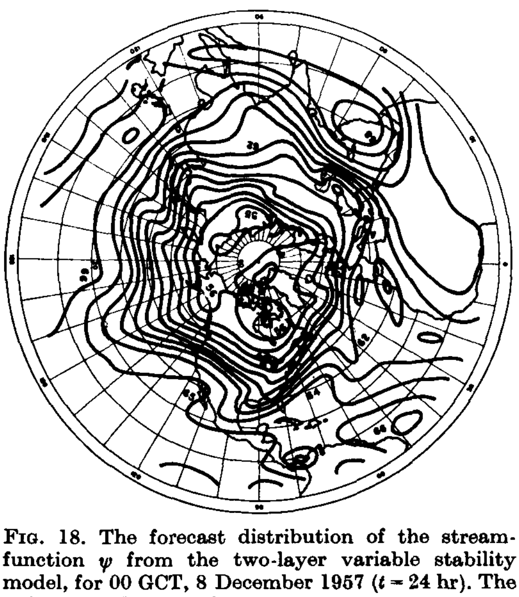

FIG. 18. The forecast distribution of the streamfunction ψ from the two-layer variable stability model, for 00 GCT, 8 December 1957 ($t=24$ hr). The units are 10^7 m^2 sec^{-1}.

FIG. 19. The forecast distribution of the vertical motion ω from the two-layer variable stability model, for 00 GCT, 8 December 1957 ($t=24$ hr). The units are mb hr^{-1}. The isolines -25, -1, 23, ... are drawn, with the area of ω more negative than -1 shaded.

of the usual two-level model, although the predicted gradients are generally more intense, and by 24 hr there is a tendency for the present model's fields to become more "ragged". If we recall that the balanced model employs the adiabatic equation without approximation, this behavior appears to be due to the inclusion of the (possibly poorly determined) temperature advection by the divergent wind. This same effect is noticeable in the predicted stability σ_{ij} distribution. This field appears more cellular than does the σ field at $t=0$ (Fig. 15), and while the stability patterns appear to be more-or-less advected by the wind field, the magnitudes of the high and low stability cells have tended to become more extreme during the 24-hr forecast. (The restriction (60), however, had to be applied at no more than five points at any one time).

The key to this evident deterioration of the two-layer balanced model's forecasts is the ω_{ij} field, shown in Fig. 19. We see at once that the field is rather irregular and of large magnitude, with a maximum ω_{ij} of 155 mb hr^{-1}, occurring over the central United States. In response to this extreme ω_{ij}, the χ_{ij} field is distorted into a two-cell distribution between North America and central Asia. While this ω_{ij} pattern shows some continuity from the

Model	t(hr)	$\{A' \cdot K'\}$	$\{K' \cdot \bar{K}\}$	$\{\bar{A} \cdot \bar{K}\}$	$\{\bar{A} \cdot A'\}$	$\{A' \cdot \bar{A}\}_1$	$\{A' \cdot \bar{A}\}_2$
Two-layer quasi-geostrophic	0	46	19	−34	38	—	—
	6	40	26	11	26	—	—
	12	32	29	36	16	—	—
	18	23	28	51	8	—	—
	24	16(42)	26(21)	21(−46)	2(26)	—	—
Two-layer balanced	0	58	−5	119	33	74	−0.1
	6	63	−9	129	34	81	−0.0
	12	63	−12	278	36	174	0.2
	18	92	−14	368	42	230	0.9
	24	183	−22	177	31	111	2.4

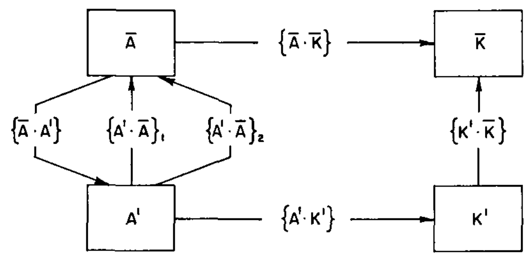

FIG. 20. The energy transformations of the two-level quasi-geostrophic and two-layer variable stability models (GATES, 1961), where A denotes available potential energy (62 or 63), K denotes kinetic energy (61), and the bar and prime denote the zonal average and perturbation, respectively. The transformations shown schematically are considered positive. The calculations given are for the initial data of 00 GCT, 7 December 1957, and for the models' 6-hourly forecast fields. The units are 10^{13} joule sec^{-1}. The values found from the verification data of 00 GCT 8 December 1957 are given in parentheses.

initial ω_{ij} distribution (Fig. 16), the χ_{ij} field does not, and neither can be considered representative of large-scale or synoptic flow. Further integration of the system with this ω_{ij} and χ_{ij} distribution would clearly introduce an increasingly large distortion of the forecasts which is evidently not present in the quasi-geostrophic case. This difficulty is probably related to the nature of the ω-equation (56), and will be discussed further in § 11.

10. Energy transformations

In addition to the foregoing examination and comparison of the models' specific numerical forecasts, it is of interest to consider their specification of the various energy transformations. For the barotropic model, only the kinetic energy of the non-divergent horizontal flow is present, and the barotropic energy cycle consists of the redistribution of this energy between, say, the zonal mean flow and the disturbances. Although this transformation was not separately computed, it appears (from the usual two-level model) that its direction is such that the (barotropic) disturbances are giving energy to the mean zonal flow in the familiar manner.

For the total kinetic energy, for all models here considered, we have

$$\int K ds = \frac{p_0}{2g}\int (\nabla\psi \cdot \nabla\psi + \nabla\tau \cdot \nabla\tau)\, ds, \qquad (61)$$

and for the total available potential energy of the two-level quasi-geostrophic model we have

$$\int A\, ds = \frac{Rp_0}{2^{\varkappa+2} g\sigma_0}\left[\int \theta^2 ds - \left(\int \theta ds\right)^2\right], \qquad (62)$$

where ds is a fractional (non-dimensional) area element with integration extending over the sphere. For the two-layer balanced model of variable static stability, the total available potential energy is given by

$$\int A\,ds = \frac{Rp_0}{2^{\varkappa+1}g} \times \left[\frac{\int \theta^2 ds - \left(\int \theta\, ds\right)^2 + \int \sigma^2 ds - \left(\int \sigma\, ds\right)^2}{\int \sigma\, ds + \left(\int \sigma\, ds\right)_m} \right], \quad (63)$$

where $(\ )_m$ denotes the maximum value under adiabatic redistribution (LORENZ, 1960). If we now partition the flow into a zonal mean (denoted by a bar) and a disturbance (denoted by a prime), we may construct the energy cycle and the associated energy transformation functions. This has been done by PHILLIPS (1954, 1956) for the two-level quasi-geostrophic model and by GATES (1961) for the two-layer balanced model, and need not be repeated here. It may be useful, however, to recall the notation introduced by Phillips according to which the symbol $\{\bar{A}\cdot A'\}$, for example, denotes the rate of change of the (total) energy of the disturbances (A') due to a transformation from the (total) energy of the zonal mean ($\bar{A}$).

The energy transformations for the two-level quasi-geostrophic model and for the two-layer balanced model were computed from the initial data as well as from the forecast data every 6 hr, and are shown in Fig. 20. In spite of the generally similar appearance of the initial fields for these two models, the initial energy transformations are quite different. In particular, we may note the entirely opposite signs of the transformation $\{K'\cdot\bar{K}\}$ and the initially opposite sense of the transformation $\{\bar{A}\cdot\bar{K}\}$ in these models. The transformation $\{A'\cdot\bar{A}\}_1$—arising from the variation of the static stability—evidently contributes significantly to the reduction of the perturbation potential energy. The relative prominence of the transformations $\{\bar{A}\cdot\bar{K}\}$ and $\{A'\cdot\bar{A}\}_1$ in both models reflects the importance of the mean meridional circulation in the energy cycle, and is, unfortunately, sensitive to the larger-scale errors which may be present in the ω solutions. In the case of the balanced model, this sensitivity has resulted in what can only be considered unacceptably large energy transformation rates by 12 hr. The quasi-geostrophic model, on the other hand, shows a monotonic decrease of the transformations $\{A'\cdot K'\}$ and $\{\bar{A}\cdot A'\}$, a decrease which continues to 72 hr. This indicates an overall under-prediction (and later reversal) of the flow of energy from the mean thermal field to the disturbances, and appears consistent with the general tendency of this model to dampen individual synoptic disturbances.

11. Further discussion and conclusions

Although only a single case has been examined, it appears that the two-layer balanced model behaves in basically the same fashion as does the more familiar two-level quasi-geostrophic model, with both models failing to predict significant baroclinic development. This probably means either: (i) that the baroclinic terms neglected in the vorticity equation in both models are important in large-scale flow and that the evolution of the vorticity field is not satisfactorily given by non-divergent winds alone, and/or: (ii) that two-levels (or layers) in the vertical are not sufficient to portray large-scale development.

The effects of a variable static stability in the two-layer balanced model evidently has little initial effect on the flow other than the approximate doubling of ω (an effect due more to the layered formulation of the model than to variable σ itself). The initial energy transformations for the balanced model, however, suggest a significantly different evolution of the disturbances, and it is unfortunate that a sufficiently well-behaved integration to document this development could not be obtained. The decay of the balanced model's forecasts clearly arises from the ω solutions well before $t = 24$ hr, and χ is simultaneously distorted. By about $t = 24$ hr the field of θ, and hence the σ field, show increasing irregularity, and no doubt shortly after this time the ψ and τ fields themselves would be noticeably affected by this instability.

In view of this behavior, it is probably worthwhile to reconsider the problem of determining ω in the balanced model. According to the continuity equation, the hemisphere-wide average ω should be zero, and this property should be approximated by the difference solution ω_{ij} as closely as possible. In the two-level quasi-geostrophic model integration to 72 hr, for example, the average ω_{ij} remained below 0.04 mb hr^{-1}, and in the two-layer balanced model integration to 24 hr ω_{ij} remained below 0.07 mb hr^{-1} until $t = 14.5$ hr and thereafter increased irregularly, reaching 0.23 mb hr^{-1} at $t = 21.5$ hr.

This erratic behavior at the larger t is probably a numerical instability introduced by the failure of the finite-difference equations to preserve with sufficient accuracy the various integral properties which are so prominent a feature of the *differential* formulation of the model. For example, total potential temperature and total vorticity are not exactly conserved by the present finite-difference version of the model, in addition to the non-conservation of mass via ω_{ij}. These initially small but persistent errors are evidently capable of serious distortion of a forecast, and particularly so in the case of ω_{ij}. An alternate formulation of the ω equation may be found by transformation of (25) using the continuity equation (28):

$$\nabla^2(\sigma\omega) = \frac{p_0}{2}\left[\nabla^2 J(\psi, \theta) + \nabla^2 J(\tau, \sigma)\right] + \left\{\frac{2^{\varkappa} p_0}{R}\nabla \cdot \left(f\nabla\frac{\partial\tau}{\partial t}\right) - \frac{p_0}{2}\nabla^2(\nabla\sigma \cdot \nabla\chi)\right\}. \quad (64)$$

This $\sigma\omega$ equation is free, we may note, of the minor restrictions placed upon $\nabla^2\sigma$ and f in (51). A finite-difference analogue of (64) might then be constructed to replace (56) which could have less truncation error in the determination of the right-hand terms than is the case in (56). The authors attempted an integration of the finite-difference analogue of (64) using the (imperfect) difference schemes discussed in § 5, but were unable to obtain convergent solutions beyond $t = 0$.

We may conclude this discussion with a few comments and suggestions for the improvement and extension of the present research effort, since it is strongly felt that further systematic comparative tests of atmospheric models is needed to document their physical differences and evaluate their forecast capabilities. Perhaps that improvement most clearly indicated by the present tests is need for better finite-difference schemes to preserve more faithfully conservative physical properties. The use of a smaller latitudinal mesh size at the higher latitudes would also be desirable to document more fully the generally smaller-scale high latitude systems. Another improvement in the model's hemisphere-wide performance would probably result from the objective rather than subjective analysis of the initial data, although it seems unlikely that the models' critical performance over the United States would be greatly affected. At several times during the course of the present work it was clear that the extrapolated Liebmann relaxation procedure was not a particularly efficient solution method on the present grid. In the two-layer balanced model, for example, approximately 300 grid scans (and 4.25 min on the 7090 computer) were required per time step to about $t = 6$ hr, with the number of required scans per time step increasing to over 1200 by $t = 24$ hr. It seems likely that a considerable saving of machine time could be effected through research on an improved relaxation method designed for the spherical grid, or by consideration of other solution methods. With the development of these and other improvements, a renewed effort in comparative model integration would be in order, and an extended test series could be expected to yield more meaningful comparisons.

Acknowledgements

The authors would like to acknowledge the cooperation and assistance of the U.C.L.A. Computing Facility in providing access to the IBM 7090 computer on which the computations were performed. Thanks are also due to Miss Marlies Oberländer for assistance in many phases of this work.

REFERENCES

Bolin, B., 1955, Numerical forecasting with the barotropic model. *Tellus*, 7, pp. 27–49.

Bolin, B., 1956, An improved barotropic model and some aspects of using the balance equation for three-dimensional flow. *Tellus*, 8, pp. 61–75.

Bolin, B., Dobrishman, E. M., Hinkelmann, K., Knighting, E., and Thompson, P. D., 1962, Numerical methods of Weather Analysis and Forecasting. *Technical Note* No. 44, World Meteorological Organization, Geneva, p. 31.

Bushby, F. H., and Hinds, M. K., 1955, Further computations of 24-hr pressure changes based on a two-parameter model. *Quart. J. Roy. Meteor. Soc.*, 81, pp. 396–402.

Bushby, F. H., and Whitelam, C. J., 1961, A three-parameter model of the atmosphere suitable for numerical integration. *Quart. J. Roy. Meteor. Soc.*, **87**, pp. 374–392.

CRESSMAN, G. P., 1958, Barotropic divergence and very long atmospheric waves. *Mon. Wea. Rev.*, **86**, pp. 283–297.

CRESSMAN, G. P., 1960, Improved terrain effects in barotropic forecasts. *Mon. Wea. Rev.*, 88, pp. 327–342.

DÖÖS, B. R., 1962, Routine numerical weather prediction in Sweden. *Proceedings of the International Symposium on Numerical Weather Prediction in Tokyo*, Meteorological Society of Japan, Tokyo, pp. 21–23.

EDELMANN, W., and REISER, H., 1962, Baroclinic forecasts with the unfiltered 5-layer model. *Technical Note* No. 5, German Weather Service, Research Division, Offenbach/M., pp. 33.

GATES, W. L., POCINKI, L. S., and JENKINS, C. F., 1955, Results of numerical prediction with the barotropic and thermotropic atmospheric models. *Geophys. Res. Paper* No. **46**, Air Force Cambridge Research Center, Cambridge, Mass., p. 168.

GATES, W. L., 1961, The stability properties and energy transformations of the two-layer model of variable static stability. *Tellus*, **13**, pp. 460–471.

GATES, W. L., 1962, Preliminary analysis of a model of self-determining static stability. *Proceedings of the International Symposium on Numerical Weather Prediction*, Meteorological Society of Japan, Tokyo, pp. 213–218.

GATES, W. L., and RIEGEL, C. A., 1962*a*, A study of numerical errors in the integration of barotropic flow on a spherical grid. *J. Geophys. Res.*, **67**, pp. 773–784.

GATES, W. L., and RIEGEL, C. A., 1962*b*, Further studies of numerical errors in the integration of barotropic flow on a spherical grid. Final Report, Contract AF19(604)-6149, Department of Meteorology, University of California, Los Angeles, 31 December 1962, p. 39.

KNIGHTING, E., and HINDS, M. K., 1960, A report on some experiments in numerical prediction using a stream function. *Quart. J. Roy. Meteor. Soc.*, **86**, pp. 504–511.

KNIGHTING, E., CORBY, G. A., BUSHBY, F. H., and WALLINGTON, C. E., 1961, An experiment in numerical forecasting. *Meteor. Office Scientific Paper* No. 5, H.M.S.O., London.

KNIGHTING, E., 1962, Numerical weather forecasting in the British Meteorological Office. *Proceedings of the International Symposium on Numerical Weather Prediction in Tokyo*, Meteorological Society of Japan, Tokyo, pp. 15–17.

LORENZ, E. N., 1960, Energy and numerical weather prediction. *Tellus*, **12**, pp. 364–373.

PHILLIPS, N. A., 1954, Energy transformations and meridional circulation associated with simple baroclinic waves in a two-layer quasi-geostrophic model. *Tellus*, **6**, pp. 273–286.

PHILLIPS, N. A., 1956, The general circulation of the atmosphere: a numerical experiment. *Quart. J. Roy. Meteor. Soc.*, 82, pp. 123–164.

SOMMERFELD, A., 1949, *Partial Differential Equations in Physics*, translated by E. G. Strauss, Academic Press, New York, p. 335 (see pp. 166–168).

Staff Members, Deutscher Wetterdienst, 1960, Barotropic forecasts with the primitive equations, Part E. *Research in Objective Weather Forecasting*, Final Report, Contract AF61 (514)-1211, Deutscher Wetterdienst, Offenbach/M., 31 December 1960.

Staff Members, Deutscher Wetterdienst, 1960, Baroclinic forecast tests with the primitive equations, Part H. *Research in Objective Weather Forecasting*, Final Report, Contract AF61 (514)-1211, Deutscher Wetterdienst, Offenbach/M., 31 December 1960.

THOMPSON, P. D., and GATES, W. L., 1956, A test of numerical prediction methods based on the barotropic and two-parameter baroclinic models. *J. Meteor.*, **13**, pp. 127–141.